# COMBINED OPERATION OF PELLET INJECTION AND LOWER HYBRID CURRENT DRIVE ON ASDEX

F.X. Söldner, V. Mertens, R. Bartiromo, H.S. Bosch, M. Kornherr,
R. Lang, F. Leuterer, R. Loch, W. Sandmann, K. Ushigusa

IPP III/167 October 1990

MAX-PLANCK-INSTITUT FÜR PLASMAPHYSIK

8046 GARCHING BEI MÜNCHEN

MAX-PLANCK-INSTITUT FÜR PLASMAPHYSIK

GARCHING BEI MÜNCHEN

# COMBINED OPERATION OF PELLET INJECTION AND LOWER HYBRID CURRENT DRIVE ON ASDEX

F.X. Söldner, V. Mertens, R. Bartiromo, H.S. Bosch, M. Kornherr,
R. Lang, F. Leuterer, R. Loch, W. Sandmann, K. Ushigusa

IPP III/167 October 1990

*Die nachstehende Arbeit wurde im Rahmen des Vertrages zwischen dem Max-Planck-Institut für Plasmaphysik und der Europäischen Atomgemeinschaft über die Zusammenarbeit auf dem Gebiete der Plasmaphysik durchgeführt.*

# COMBINED OPERATION OF PELLET INJECTION AND LOWER HYBRID CURRENT DRIVE ON ASDEX

F.X. Söldner, V. Mertens, R. Bartiromo[1], H.S. Bosch, M. Kornherr, R. Lang,
F. Leuterer, R. Loch, W. Sandmann, K. Ushigusa[2]

Max-Planck-Institut für Plasmaphysik, EURATOM Association
D-8046 Garching, Fed. Rep. of Germany

## ABSTRACT

Simultaneous operation of Lower Hybrid-current drive and pellet injection could be successfully achieved. With peripheral ablation of the pellets by suprathermal electrons, the same net inward flux of particles is found as with deep penetration of pellets into ohmically heated plasmas. The density profile $n_e(r)$ peaks with the same increment of the peaking factor $Q_n = n_{eo} / < n_e >$ in both cases. The global energy confinement time rises with density, $\tau_E \sim \bar{n}_e$, in the combined operation.

---

[1]ENEA, Frascati, Italy

[2]Naka Fusion Research Establishment, JAERI, Naka, Japan

## INTRODUCTION

Lower Hybrid (LH) waves are successfully used for current drive and heating at low density. Their application at high density is impaired by the problem of wave accessibility to the central plasma region and may be impeded by power depletion near the plasma edge through nonlinear processes such as parametric decay instabilities. Efficient heating at high density was achieved by launching LH waves into plasmas with peaked density profiles /1/. Peaking of the density profile is routinely obtained with particle fuelling by pellet injection /2/. This also provides superior energy confinement /3/. Combination of pellet injection and LH waves might therefore allow current drive and heating in the central region of high-density plasmas with good overall confinement properties. The first successful experiments with simultaneous operation of LH-current drive (LHCD) and pellet injection are reported in this paper.

## PELLET ABLATION WITH LOWER HYBRID

Multiple pellet injection is performed on ASDEX with a centrifuge delivering up to 80 pellets during a single discharge with velocities of up to 600 m/s /4/. In the combined experiments with LH, deuterium pellets were injected into deuterium discharges with a repetition rate of 17-25 Hz. Two different sizes were used: with particle number $N \approx 4 \times 10^{19}$ and a velocity v=200 m/s, and with $N \approx 6 \times 10^{19}$ particles and v=400 m/s, both with diameter $\varnothing$ = 1 mm. To investigate the pellet ablation process, the emitted $H_\alpha$ radiation is monitored with fast diodes. Information about the spatial distribution of the ablation is obtained from photographs taken through narrow band interference filters at the $H_\alpha$ line. In ohmic target plasmas the pellets of the smaller size penetrate to about half the plasma radius. The ablation profile for these conditions is plotted in Fig. 1a. In combined experiments with LH, pellet injection is started at low initial density, where the LH-current drive efficiency is high /5/. The ablation is then dominated by suprathermal electrons, and the mass deposition profile strongly depends on the LH wave spectrum. With LH-current drive at low $N_{||}$ ( $\overline{N}_{||}$=1.8, $\Delta\varphi$ =75°), the pellets are ablated in a narrow zone near the plasma periphery, as seen from the sharp peak close to the separatrix in Fig. 1b. LH waves with high phase velocities produce suprathermal electrons with a mean energy of $E_S \approx 70$ keV under these conditions /6/. Such high-energy electrons can cause decomposition and ablation of the pellets in a short time due to the absorption of the fast electrons in the interior of the pellets /7/. The gas cloud arising from the evaporation of the solid pellet expands along the torus and results in an additional broad wing of the $H_\alpha$ signal in Fig. 1b. With LH waves of higher $N_{||}$, the

pellets are ablated further inside the separatrix, as shown in Fig. 1c. In this case a symmetric LH spectrum with $\overline{N}_{||}$=4.4 ($\Delta\varphi$=180°) was launched. The LH waves of lower phase velocity generate fast electrons with lower mean energy which are then less efficient for fast pellet evaporation. Peripheral ablation of pellets raises the edge density and allows improved coupling of LH waves with low reflection at a large distance between the plasma boundary and the LH antenna /8/.

Penetration of pellets during LH application is rather insensitive to pellet size and velocity. The penetration depth as function of the actual density is shown in Fig. 2 for pellets with v=200, 400, 600 m/s, respectively and two different sizes, injected into ohmic and LH target plasmas. Nearly no density dependence is seen in ohmic plasmas. With LH, the density build-up with pellets reduces the population of suprathermal electrons and enables increasingly deeper penetration. The faster rise of penetration length with density in the discharge #29960 results from pellet injection after switch-off of the LH.

Pellet injection after the end of the LH pulse can probe the radial distribution of suprathermal electrons and its temporal evolution. Studies with single pellets after LH application had already been carried out on ASDEX with the previous LH system at 1.3 GHz /9/. For multiple pellet injection after LH-current drive at low $N_{||}$ ($\overline{N}_{||}$ =1.8, $\Delta\phi$=75°) the evolution of line-averaged density $\overline{n}_e$ , loop voltage $U_l$ , hard and soft X-ray emission is shown in Fig. 3. The density rises only in small steps for pellets injected briefly after LH. The number of suprathermal electrons is still large in this phase, as seen from the high level of soft X-ray radiation. The loop voltage returns to the ohmic level about 50 ms after switch-off of the LH. At this time the plasma current is carried again by thermal electrons. The hard X-ray radiation originating from MeV-runaway electrons begins to rise about 100 ms after end of the LH, when suprathermal electrons are still present and the loop voltage has reached already the higher ohmic value. Suprathermal electrons disappear completely only about 200 ms after the end of LH. At this time the soft X-ray emission has decreased to the ohmic level. The density then rises also in larger steps upon injection of pellets. The location of the mass deposition of pellets with multiple injection during the decay phase of the suprathermal electrons is plotted in Fig. 4 as a function of the delay time between turn-off of the LH and start of pellet injection. Penetration of the first few pellets after the LH pulse is still shallow. Only about 100 ms after the LH pulse does the ablation profile resemble the ohmic profile, but the penetration depth at this time is still shorter with $\Delta/a \approx 0.25$. With a delay of 200 ms to the end of the LH pulse, pellets again penetrate to the same region as in the preceding ohmic phase. The time delay for recovery of deep pellet penetration corresponds to the slowing-down time of 300 keV electrons at a density

of $n_e = 2 \times 10^{13}$ $cm^{-3}$. This is compatible with the tail distribution of LH-generated suprathermal electrons ranging up to about 500 keV, as determined from hard X-ray measurements. Collisional deceleration of the fast electrons is also counteracted by the rise of the toroidal dc electric field after end of the LH pulse. The critical velocity for the formation of runaway electrons is thereby lowered. Some of the suprathermal electrons then pass into the runaway region and are further accelerated to higher energies. This is seen from the continuous rise of the hard X-ray emission in this phase. The bursts in hard X-ray radiation after injection of each pellet indicate increased losses of the fast electrons. Pellets are not stopped by the high-energy runaway electrons in the MeV range /7/. The high-energy runaway electrons therefore do not impair pellet penetration. But suprathermal electrons up to the highest energy still absorbed within the pellets have to be slowed down before central mass deposition can be achieved again.

## DENSITY BUILD-UP DURING LH-CURRENT DRIVE

Pellet injection is started in steady-state phases of discharges, where most of the plasma current is driven by the LH waves. For this purpose the electron density is kept low in order to have high current drive efficiency. The evolution of various global plasma parameters for pellet injection during LHCD with $P_{LH}$=620 kW at $\overline{N}_{||}$=1.8 is shown in Fig.5. The line-averaged density $\overline{n}_e$ increases from an initial value of $\overline{n}_e = 1.7 \times 10^{13}$ $cm^{-3}$ immediately after injection of each pellet and continues to rise after the initial jump, indicating the inward flow of particles from the gas clouds formed through pellet evaporation near the plasma periphery. For later pellets, $\overline{n}_e$ remains on successive flat-top levels and decays only slowly after the end of pellet injection. The density profile $n_e(r)$, first flattened during the gas-puff-fuelled LHCD phase gradually peaks during pellet injection, with the profile factor $Q_n = n_{eo} / < n_e >$ rising from ~1.4 to ~1.8. In spite of the shallow penetration of the pellets and the peripheral mass deposition during LH application, a strong inward flow of particles leads to an increase of the central density as in experiments with deep pellet ablation. With pellet injection into ohmic target plasmas of similarly low initial density, the line-averaged density $\overline{n}_e$ decays after the initial jump following each pellet, as shown in Fig. 6, upper case. The density profile there starts peaking only in a late phase at t≈2.05 s, 800 ms after the start of pellet injection. At this time sawteeth disappear, as seen from the density trace.

In the LHCD discharge documented in Fig.5, sawteeth are suppressed immediately after the start of the LH pulse. This can be seen from the soft X-ray emission, plotted in Fig.7 for two lines of sight. The strong rise in the signals with the start of LH at

t=1s originates from the emission of the LH-generated suprathermal electrons. The signals drop slightly after injection of each pellet due to the transient depletion of fast electrons in the pellet ablation process. After suppression of the sawtooth oscillations, the m=1 mode grows to large amplitude, as usually observed with LH-current drive on ASDEX /10/. This MHD activity is seen on the line-integrated signal from a central chord of the soft X-ray camera (Fig. 7, upper case). In a late phase after the last pellet, at t≈1.6 s, the m=1 mode is weakened and finally stabilized. In the subsequent MHD-quiescent phase, the line-averaged density $\bar{n}_e$ stays nearly constant and the density profile peaks strongly. Also the radial profile of soft X-ray emission peaks. The neutron emission then rises by a factor of about 2 (Fig. 5, center). This phase of improved central particle confinement is finished abruptly by the onset of sawtooth oscillations at t≈1.8 s with one major crash.

## ENERGY CONFINEMENT

The confinement behaviour of pellet-fuelled ohmic and LH-driven discharges is compared in a density range covering linear and saturated confinement regimes of gas puff-fuelled ohmic discharges. The total energy content, as obtained from magnetic measurements, and the thermal electron energy content determined from Thomson scattering, increase with pellet injection in the cases of both ohmic and LHCD target plasmas. The corresponding $\beta_p$ values are shown in Figs.5 and 6, center cases. With LHCD, $\beta_p^{equ}$ is larger than $\beta_p^{dia}$ due to the pressure anisotropy originating from the suprathermal electron distribution. The difference between the increments in $\beta_p^{dia}$ and $\beta_p^{equ}$ disappears with rising density due to the weaker anisotropy of the electron distribution at higher density. There the electron heating is slightly reduced, as seen from saturation of $\beta_p{}^{el}$. But during this period ion heating is enhanced and leads to a strong rise in neutron production. With rising density the current drive efficiency diminishes and the residual ohmic power input required for maintaining the total plasma current at its flat-top value slowly rises, as seen from Fig. 5, lower case. The energy confinement time $\tau_E$ drops first after the start of LH, as the total heating power increases. For LH the same inverse power scaling of $\tau_E$ has been found as for other additional heating methods /11/. With begin of pellet injection, $\tau_E$ starts to rise although the total power input increases due to the rise in ohmic power. For the calculation of $\tau_E$ an experimentally determined density-dependent absorption coefficient $\alpha$ for the LH power is used /12/. The energy confinement time then rises with density during the pellet-fuelled phase of the LH-driven discharge in the same way as with pellet injection into ohmic target plasmas (Fig.6, lower case). With LH application to gas-fuelled

discharges with comparable plasma parameters, smaller beta values were obtained. No density dependence of the energy confinement time $\tau_E$ was found there. For the two cases of pellet injection into ohmic and into LHCD target plasmas the density dependence of the energy confinement time $\tau_E$ is shown in Fig.8. An increase of the energy confinement time with density can be regained also for LHCD plasmas by peaking the density profile with pellet injection.

LH waves were launched with different $N_{||}$ spectra, in current drive ($\overline{N}_{||}$=1.8, $\Delta\varphi$ =90° and $\Delta\varphi$ =-90°), symmetric ($\overline{N}_{||}$=4.4, $\Delta\varphi$ =180°) and compound operation (90°+180°). In the density range $\overline{n}_e$= 1.3-4 x $10^{13}$ $cm^{-3}$ the global confinement time (assuming $\alpha$=1) spreads by a factor of 2, depending on the $N_{||}$ spectrum. The highest values of $\tau_E$ are obtained with low-$N_{||}$ current drive spectra, the lowest with high-$N_{||}$ symmetric spectra. The absorption coefficient $\alpha$ of the LH power, however, also depends on the $N_{||}$ spectrum in this density range /12/. The $N_{||}$ dependence of $\tau_E$ vanishes for high-$N_{||}$ and compound spectra if only the absorbed power is taken into account by using the experimental values for $\alpha$. The energy confinement times calculated with total absorbed power are plotted versus density for the different $N_{||}$ spectra in Fig. 9. The higher confinement times with the 90° spectrum at low density are due to the larger energy content in the suprathermal electron population and also to suppression of m=1 modes. With increasing density the fraction of suprathermal electrons decreases. For these experiments with high LH power ( $P_{LH,net}$ = 1.2 MW), $\tau_E$ becomes independent of $\overline{n}_e$ for all $N_{||}$ spectra above $\overline{n}_e$= 3.5 x $10^{13}$ $cm^{-3}$, as it was observed in gas-fuelled discharges.

With injection of larger-size pellets (N≈6 x $10^{19}$ particles, v=400 m/s), the density was increased to $\overline{n}_e$ > 1 x $10^{14}$ $cm^{-3}$ during LH. At high density with $\overline{n}_e$ >7.5 x $10^{13}$ $cm^{-3}$, a further increase of $\beta_p$ and of the energy confinement time are observed. In this phase the central electron temperature decreases strongly (from 1.3 keV to 0.5 keV) due to the strong rise in central density (3 x $10^{13}$ $cm^{-3}$ to 1.5x $10^{14}$ $cm^{-3}$ ). The central ion temperature becomes equal to the electron temperature. The ion energy spectrum measured with the neutral charge exchange analyzer stays thermal and corresponds to a single Maxwellian distribution. No increase in the flux of higher energy ions is seen in the measured range of E ≤ 6 keV. Direct ion acceleration by the LH waves therefore seems not to contribute to the observed heating. It has to be rather attributed to the suppression of sawteeth and m=1 modes occuring in this phase. The soft X-ray emission profile and the density profile $n_e(r)$ then peak and the central confinement is improved, as in pellet-fuelled ohmic discharges and in LHCD discharges at low density.

## PARTICLE TRANSPORT

A well-known common feature of pellet-fuelled discharges is the strong peaking of their electron density profiles. Pellet injection into LHCD discharges exhibits a somewhat lower, but noticeable, enhancement of the central profile peaking of ~35% (see Fig. 10) compared with ~ 50 % of the corresponding ohmically heated case. This is especially remarkable since during LH injection the deposition zone of the pellet particles is shifted outward close to the plasma boundary, where also conventional gas-puff refuelling takes place.

The flattening of the steady-state profile in the central region during LH alone, as seen in Fig. 10, is correlated to the low toroidal electric dc field when most of the plasma current is driven by LH waves /13/. At higher densities $\overline{n}_e = 3.5 \times 10^{13}$ cm$^{-3}$ when the loop voltage rises again, central peaking develops.

The particle transport was determined at medium densities during the final density profile peaking phase after pellet injection for ohmic and LHCD target plasmas. Typical profiles $n_e(r)$ and the related particle fluxes averaged over one pellet cycle of ~60 ms are plotted in Fig.11. Approximately the same net inward flux of particles is found during the density build-up with peripheral pellet ablation during LH as with the deeper penetration into ohmic target plasmas. If a radially constant diffusion coefficient D and an inward velocity V linearly increasing with minor radius r are assumed, the central profile evolution can be satisfactorily reproduced by the following coefficients:

$D_{bulk}(m^2/s) = 0.05$ (**OH**) / $0.056$(**LH**) $\qquad$ $V(r/a=0.5)(m/s) = -0.38$ (**OH**) / $-0.25$ (**LH**).

The accuracy of the deduced coefficients is estimated at +/- 25 %. The analysis indicates that the inward pinch in the central region is slightly reduced by applying LHCD. This seems to be correlated to the lowered toroidal electric dc field during LH-current drive. The bulk diffusion coefficient is about the same for pellet injection into ohmic target plasmas and in combination with LHCD. For both cases it is strongly reduced in comparison with purely gas-fuelled discharges - but it is still an order of magnitude larger than the neoclassical value /13/. The central particle confinement is therefore clearly improved also with shallow pellet refuelling in combination with LH-current drive.

**SUMMARY**

Pellets are ablated near the plasma boundary in the presence of a large population of suprathermal electrons during LH-current drive. A gaseous cloud rapidly expands after decomposition of the pellets by absorption of the energy of fast electrons. The fuelling therefore resembles more fast gas puffing, with the ionization zone shifted deeper inside the plasma. In spite of the peripheral mass deposition, however, the same radial inward flow of particles is obtained as with deep fuelling by pellet injection into ohmic target plasmas. Peaking of the density profile and improvement of central and global confinement are also achieved in combined operation of pellet injection and LH-current drive. The dominant role of the m=1 mode for central particle and energy confinement has been demonstrated. With LH-current drive, sawtooth oscillations and the m=1 instability can be separated /10/. In sawtooth-free discharges during LH-current drive, strong peaking of the electron density profile and enhanced neutron production are obtained after stabilization of the m=1 mode in a late phase of pellet injection. A wide density range could be covered with pellet injection during LH application. Sophisticated scenarios with intermittent launching of LH power do not seem necessary. This could ease the combined operation of pellet injection and Lower Hybrid current drive on future large-size machines.

The Lower Hybrid experiments on ASDEX are conducted in collaboration between IPP Garching, ENEA Frascati and PPPL Princeton.

## REFERENCES


/1/ Yoshino, R., et al., IAEA Workshop on Pellet Injection and Toroidal Confinement, Ising 1988, 27.

/2/ Kaufmann, M., et al., Nuclear Fusion 28, 827 (1988).

/3/ Mertens, V. , 17th Europ. Conf. on Contr. Fusion and Plasma Physics, Amsterdam 1990, to be published.

/4/ Mertens, V. , et al., 15th Europ. Conf. on Contr. Fusion and Plasma Physics, Dubrovnik 1988, Vol. 1, 39.

/5/ Leuterer, F., et al., 17th Europ. Conf. on Contr. Fusion and Plasma Physics, Amsterdam 1990, Vol. III, 1291.

/6/ Leuterer, F., et al., Internal Report IPP III / 154, Garching (1990).

/7/ Pégourié, B., Y. Peysson, 17th Europ. Conf. on Contr. Fusion and Plasma Physics, Amsterdam 1990, Vol. III, 1227.

/8/ Leuterer, F., et al., 17th Europ. Conf. on Contr. Fusion and Plasma Physics, Amsterdam 1990, Vol. III, 1287.

/9/ Büchl, K., et al., Nuclear Fusion 27, 1939 (1987).

/10/ Söldner, F.X., et al., 17th Europ. Conf. on Contr. Fusion and Plasma Physics, Amsterdam 1990, Vol. III, 1323.

/11/ Söldner, F.X, et al., 13th Int. Conf. on Plasma Physics and Controlled Nuclear Fusion Research, IAEA-CN-53 / E-1-1, Washington (1990).

/12/ Bartiromo, R., et al., 17th Europ. Conf. on Contr. Fusion and Plasma Physics, Amsterdam 1990, Vol. III, 1092.

/13/ Gehre, O., et al., 17th Europ. Conf. on Contr. Fusion and Plasma Physics, Amsterdam 1990, Vol. I, 70.

## FIGURE CAPTIONS

Fig.1: Ablation profiles for pellet injection into an ohmic target plasma (**a**) and in combination with LH: low-$N_{||}$ current drive (**b**), and high-$N_{||}$ symmetric wave spectrum (**c**). $B_t$ = 2.3 T, $I_p$ = 300 kA for all discharges. The dashed line indicates the position of the separatrix.

Fig.2: Pellet penetration versus density for multiple injection of pellets with different size and velocity into LHCD and ohmic target plasmas.
LH wave spectra: 75°: + (680 KW), ▲(620 kW); 90°: ●(680 kW), Δ(1.2 MW); 180°: ∇(1.2 MW), 90°+180°: ◇(1.2 MW), -90°+180°: ❑(1.2 MW).

Fig.3: Temporal evolution of line-averaged density $\bar{n}_e$ , loop voltage $U_l$ , hard X-ray emission $I_{HX}$ and soft X-ray emission $I_{SX}$with multiple pellet injection after switch-off of LH-current drive with $P_{LH}$ = 680 kW, $\bar{N}_{||}$ =1.8, $\Delta\phi$=75°.

Fig.4: Variation of the pellet penetration depth with the delay between switch-off of the LH and injection of the pellet. $B_t$ = 2.3 T, $I_p$ = 300 kA, $\bar{n}_e = 2 \times 10^{13}$ cm$^{-3}$, $P_{LH}$ = 680 kW, $\bar{N}_{||}$ = 1.8.

Fig.5: Temporal evolution of various plasma parameters for a discharge with pellet injection during LH-current drive ($P_{LH} \approx$ 620 kW, $\bar{N}_{||}$ = 1.8, $\Delta\varphi = 75^{\circ}$). $B_t$ = 2.3 T, $I_p$ = 300 kA.

Fig.6: Temporal evolution of various plasma parameters for a discharge with pellet injection into an ohmic target plasma of low initial density.

Fig.7: Line-integrated soft X-ray emission from two lines of sight, through the central region and near the q=1 surface, for the discharge documented in Fig. 3.

Fig.8: Density dependence of the energy confinement time $\tau_E$ for pellet injection into the LHCD and ohmic target plasmas of Figs. 3 and 4.

Fig.9: Energy confinement times calculated with total absobed power versus density for multiple pellet injection starting at initial low density $\bar{n}_e = 1.4 \times 10^{13}$ cm$^{-3}$ during LH application with different $N_{||}$ spectra. $P_{LH}$ = 1.2 MW.

Fig.10: Normalized density profiles during LHCD with pellet fuelling (solid line) and with gas-puff fuelling (dashed), and during a standard ohmic discharge (dotted curve). The arrow at r = 0.35 m indicates the pellet penetration depth.

Fig.11: Radial profiles of the electron density and the particle flux for pellet injection into ohmic (lower case) and LHCD (upper case) target plasmas. $B_t$ = 2.3 T, $I_p$ = 300 kA.

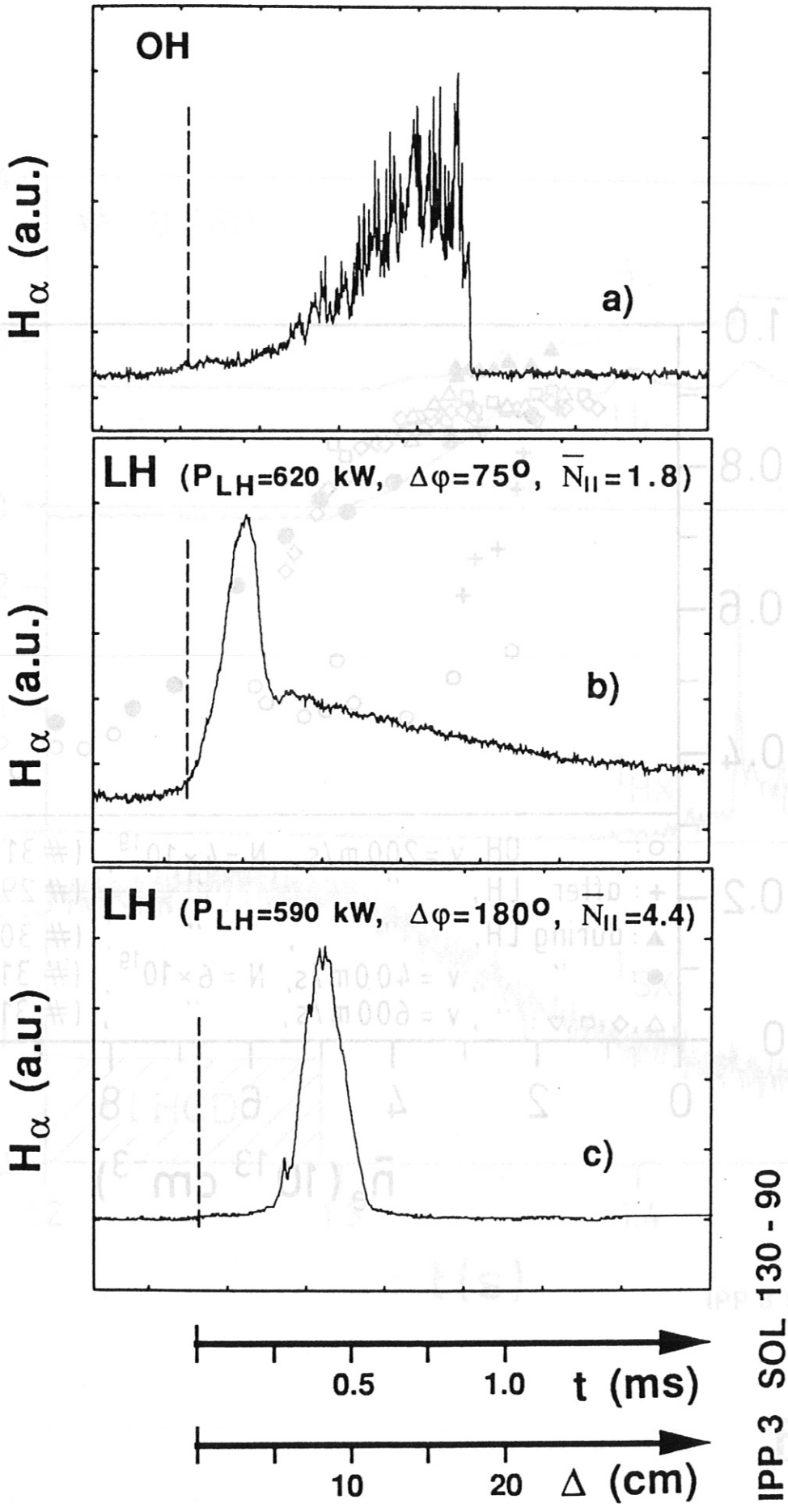
OH
$H_\alpha$ (a.u.)
a)
LH ($P_{LH}$=620 kW, $\Delta\varphi$=75°, $\bar{N}_{II}$=1.8)
$H_\alpha$ (a.u.)
b)
LH ($P_{LH}$=590 kW, $\Delta\varphi$=180°, $\bar{N}_{II}$=4.4)
$H_\alpha$ (a.u.)
c)
0.5
1.0
t (ms)
10
20
Δ (cm)
IPP 3 SOL 130 - 90

**Fig.1**

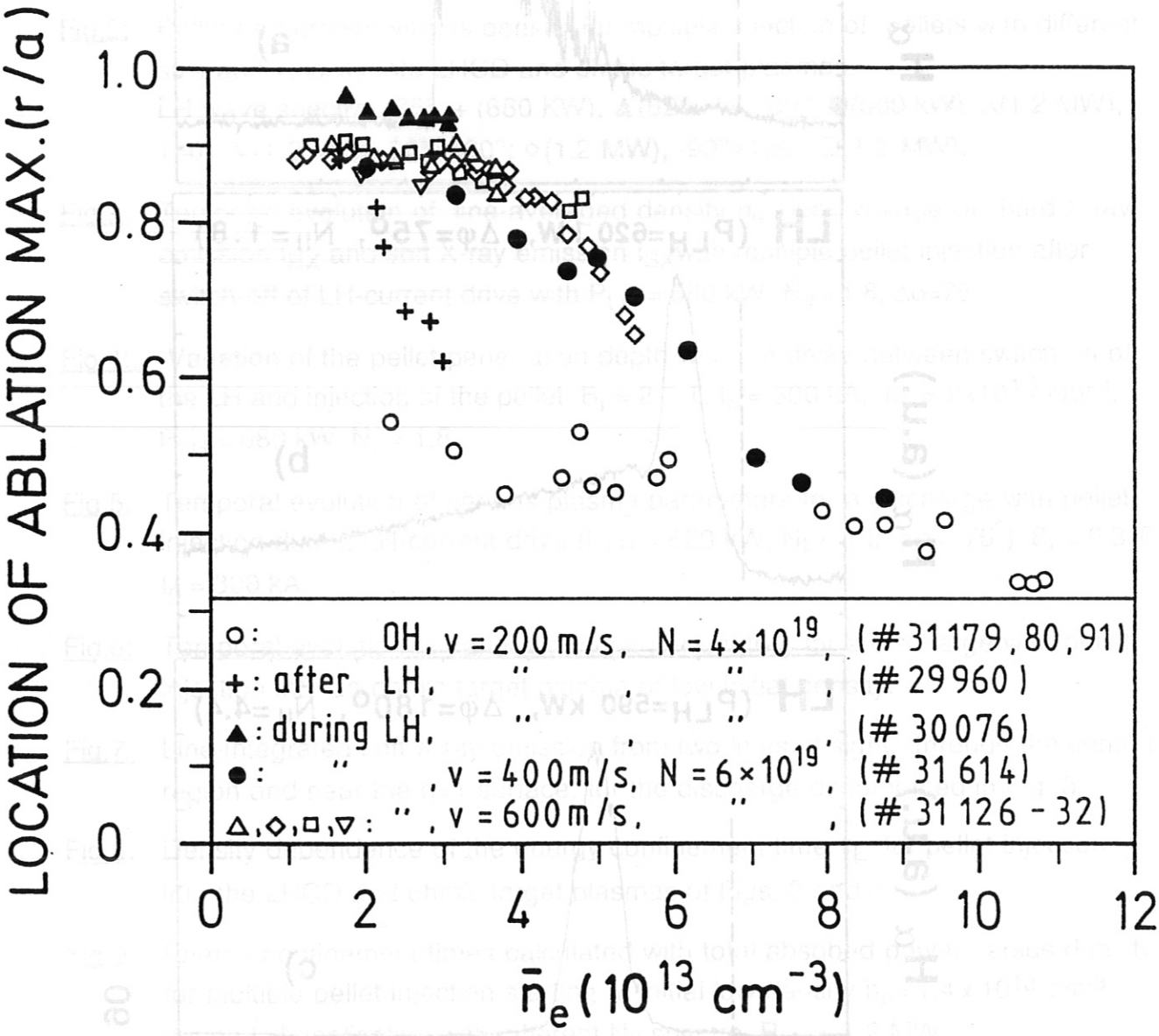
LOCATION OF ABLATION MAX.(r/a)
1.0
0.8
0.6
0.4
0.2
0
0
2
4
6
8
10
12
$\bar{n}_e$ ($10^{13}$ cm$^{-3}$)
○: OH, v = 200 m/s, N = $4\times10^{19}$, (# 31179, 80, 91)
+: after LH, " , " , (# 29960)
▲: during LH, " , " , (# 30076)
●: " , v = 400 m/s, N = $6\times10^{19}$, (# 31614)
△, ◇, □, ▽: " , v = 600 m/s, " , (# 31126 - 32)

**Fig.2**

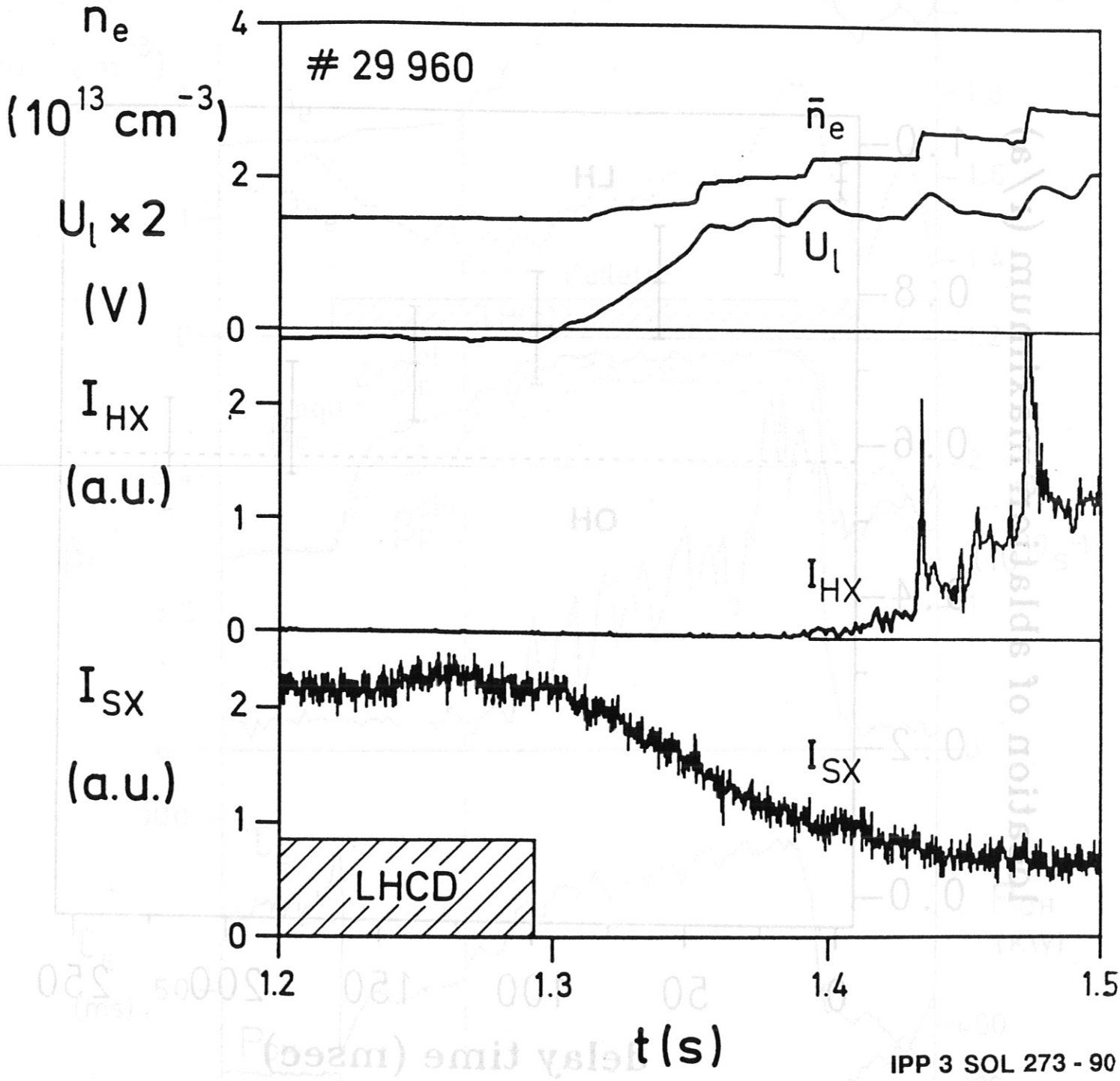
$\bar{n}_e$
$(10^{13}\,cm^{-3})$
$U_l \times 2$
(V)
$I_{HX}$
(a.u.)
$I_{SX}$
(a.u.)
# 29 960
$\bar{n}_e$
$U_l$
$I_{HX}$
$I_{SX}$
LHCD
4
2
0
2
1
0
2
1
0
1.2
1.3
1.4
1.5
t (s)
IPP 3 SOL 273 - 90

**Fig.3**

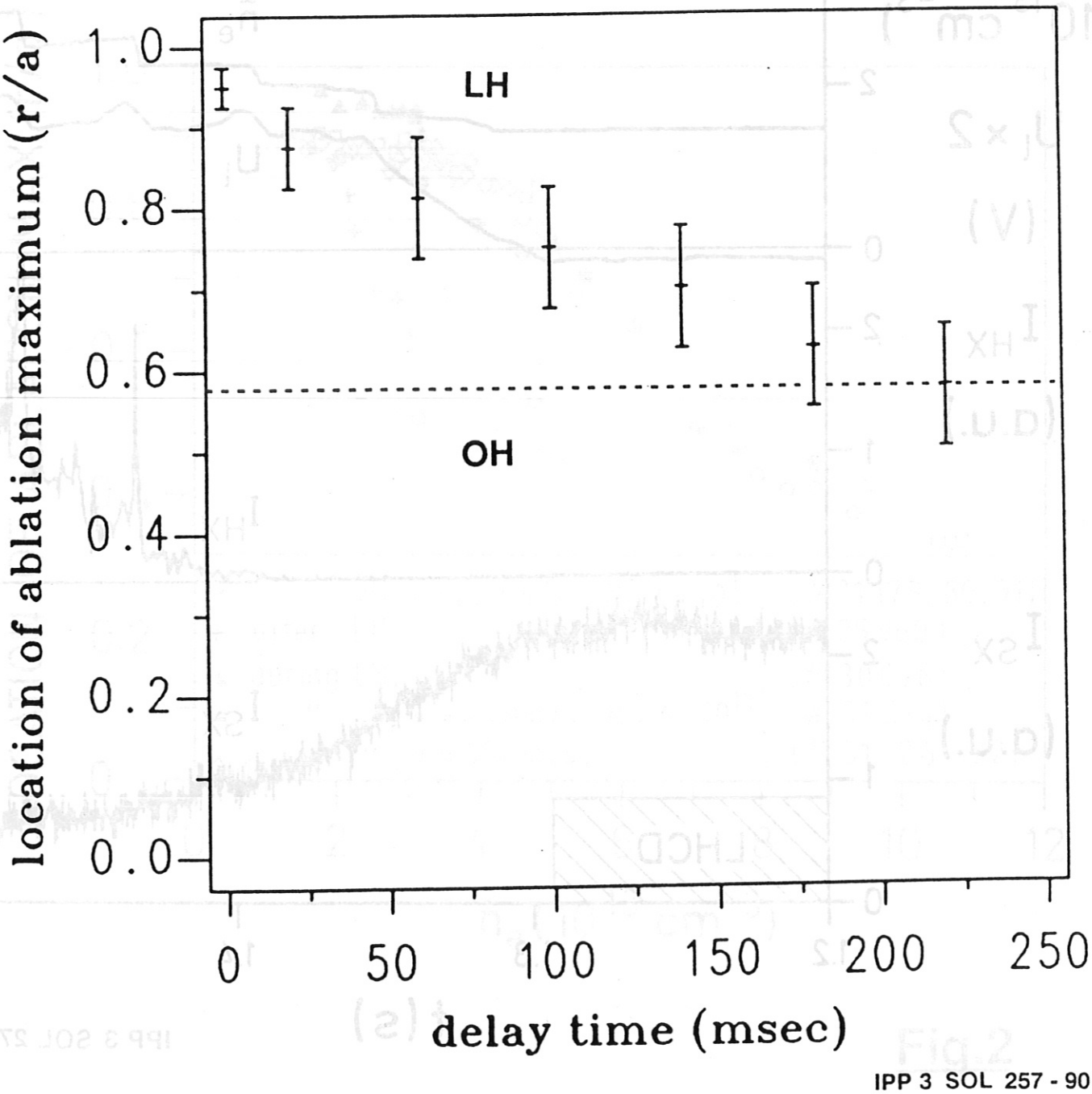


IPP 3 SOL 257 - 90

**Fig.4**

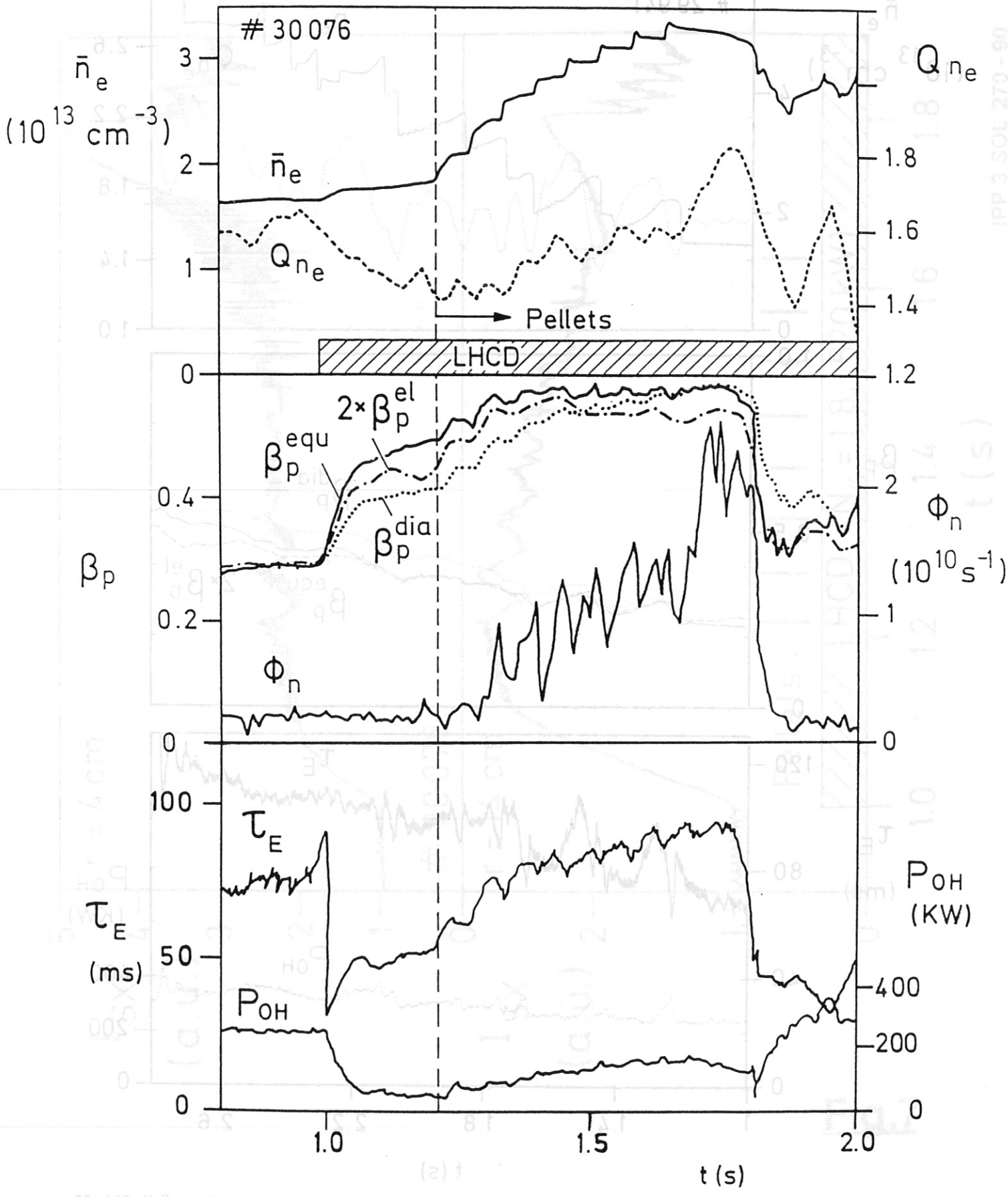


IPP 3 SOL 268 - 90

**Fig.5**

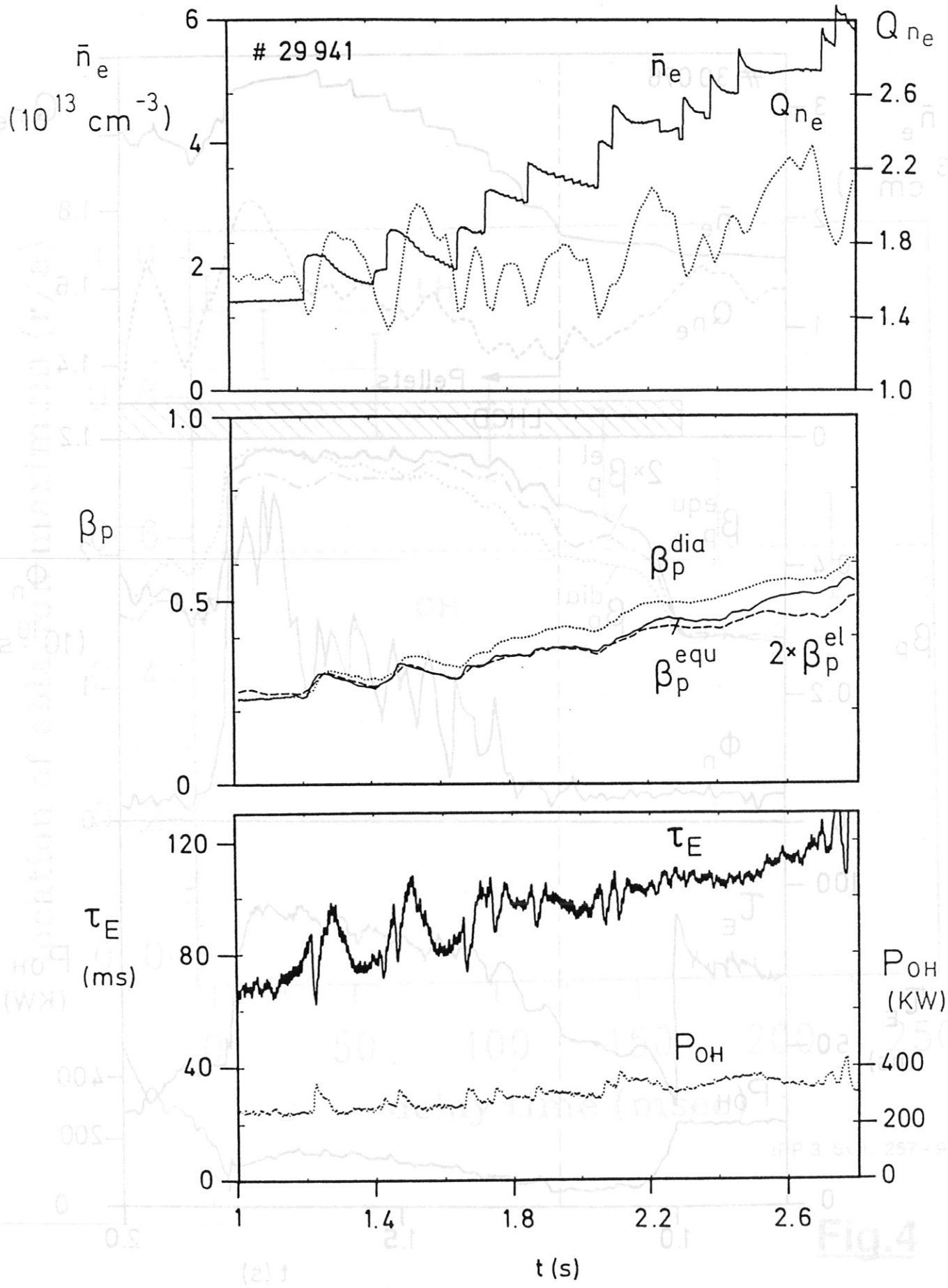


IPP 3 SOL 254 - 90

**Fig.6**

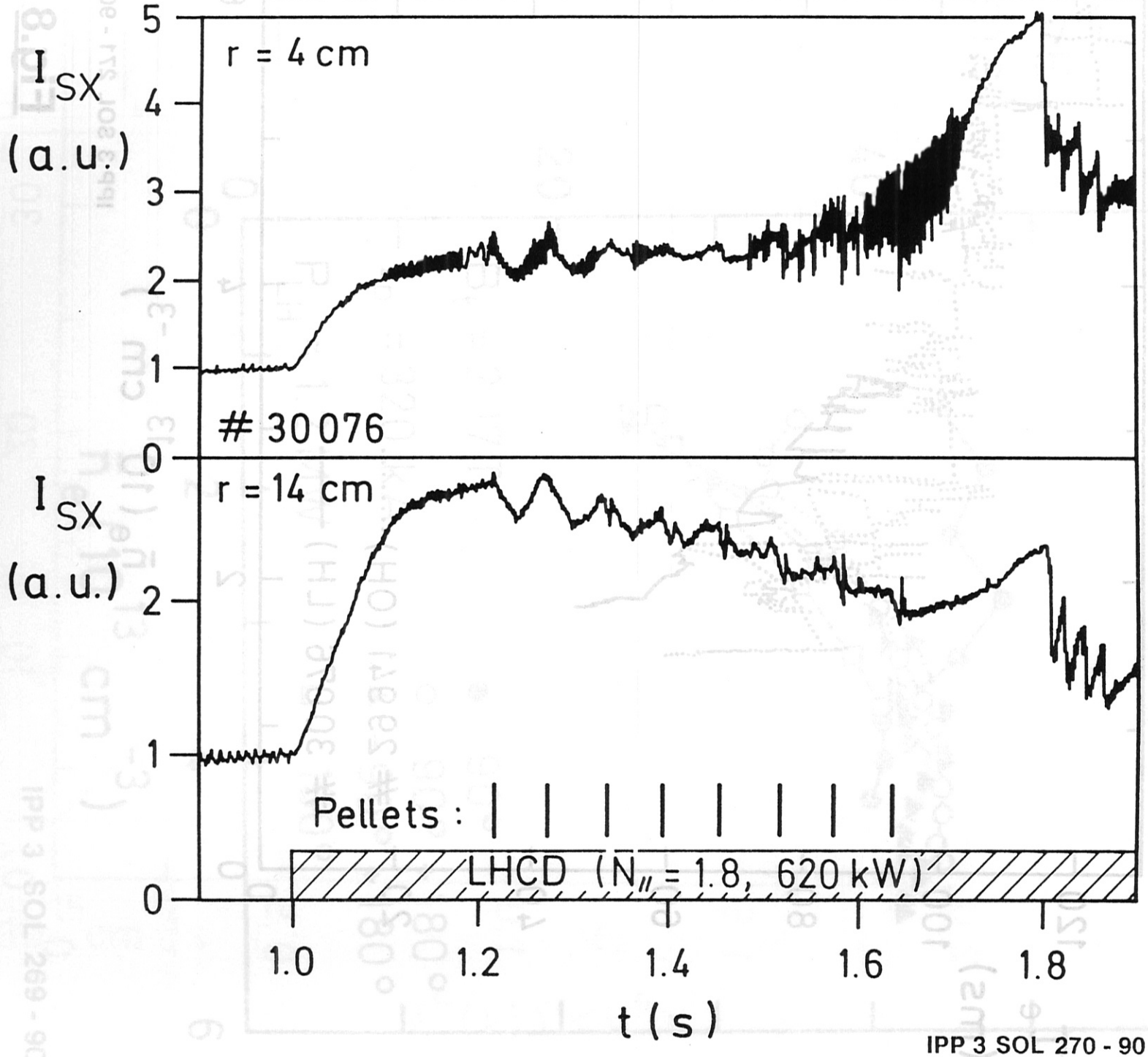


Fig.7

IPP 3 SOL 270 - 90

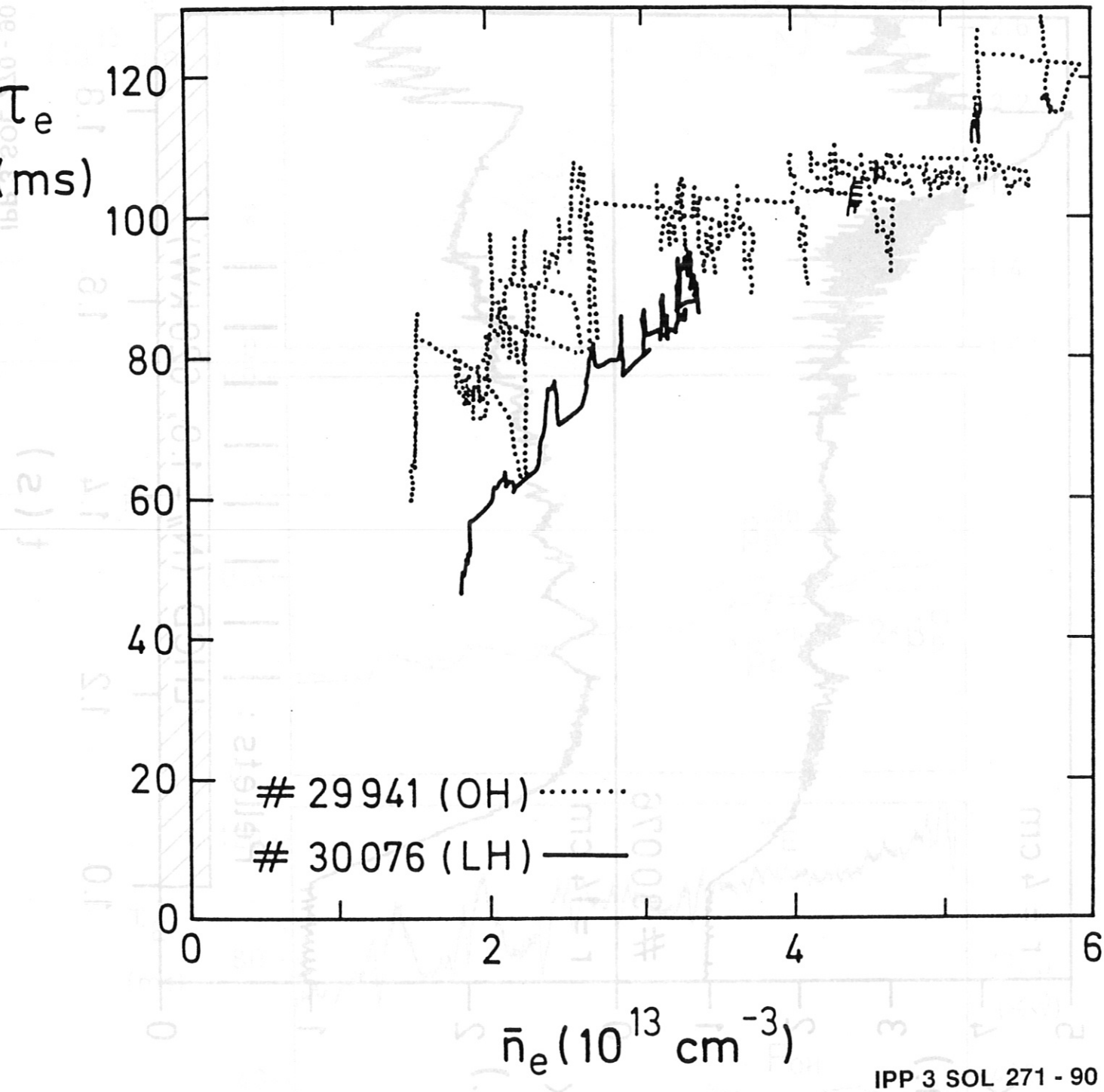


IPP 3 SOL 271 - 90

**Fig.8**

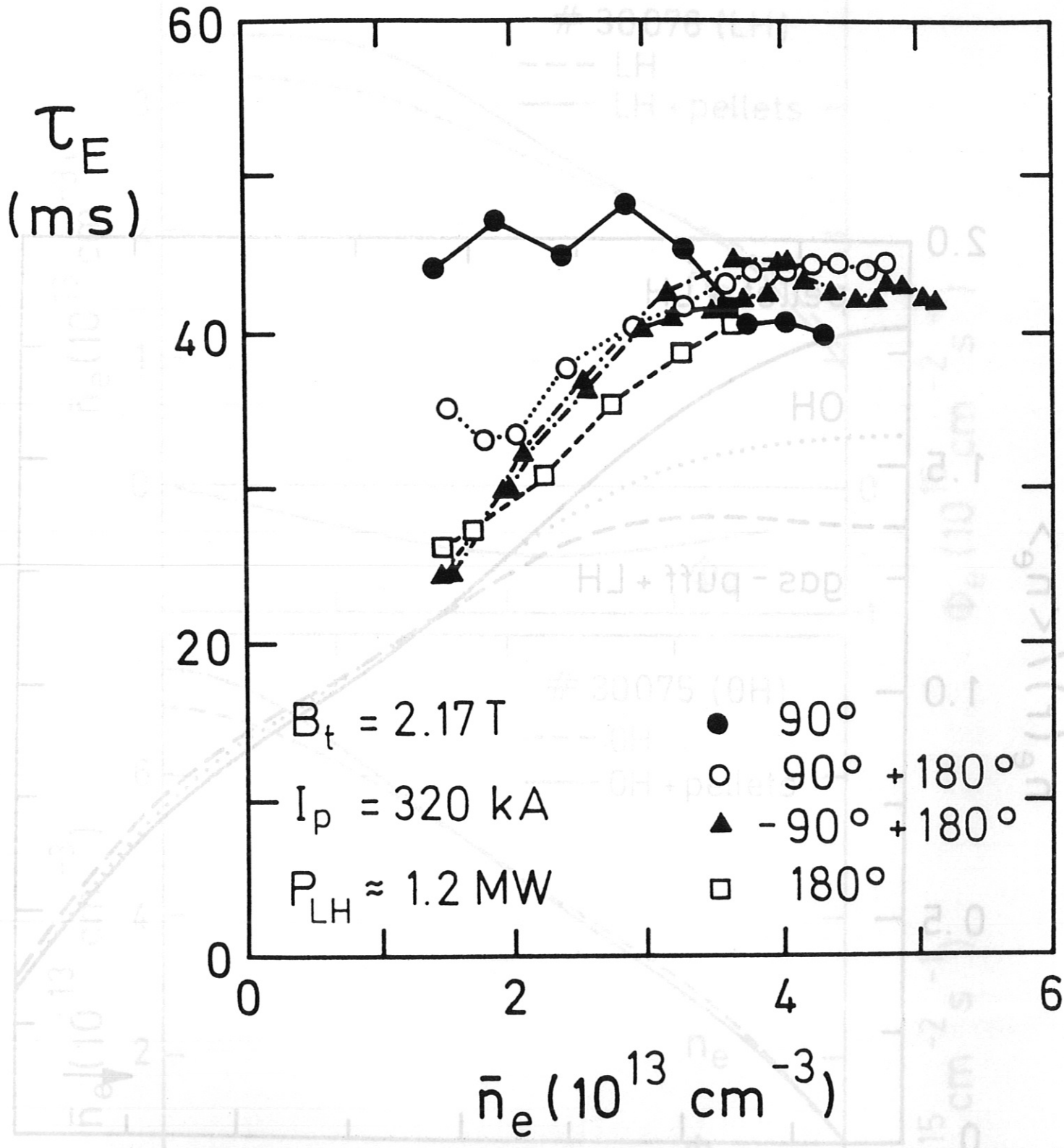


IPP 3 SOL 269 - 90

**Fig.9**

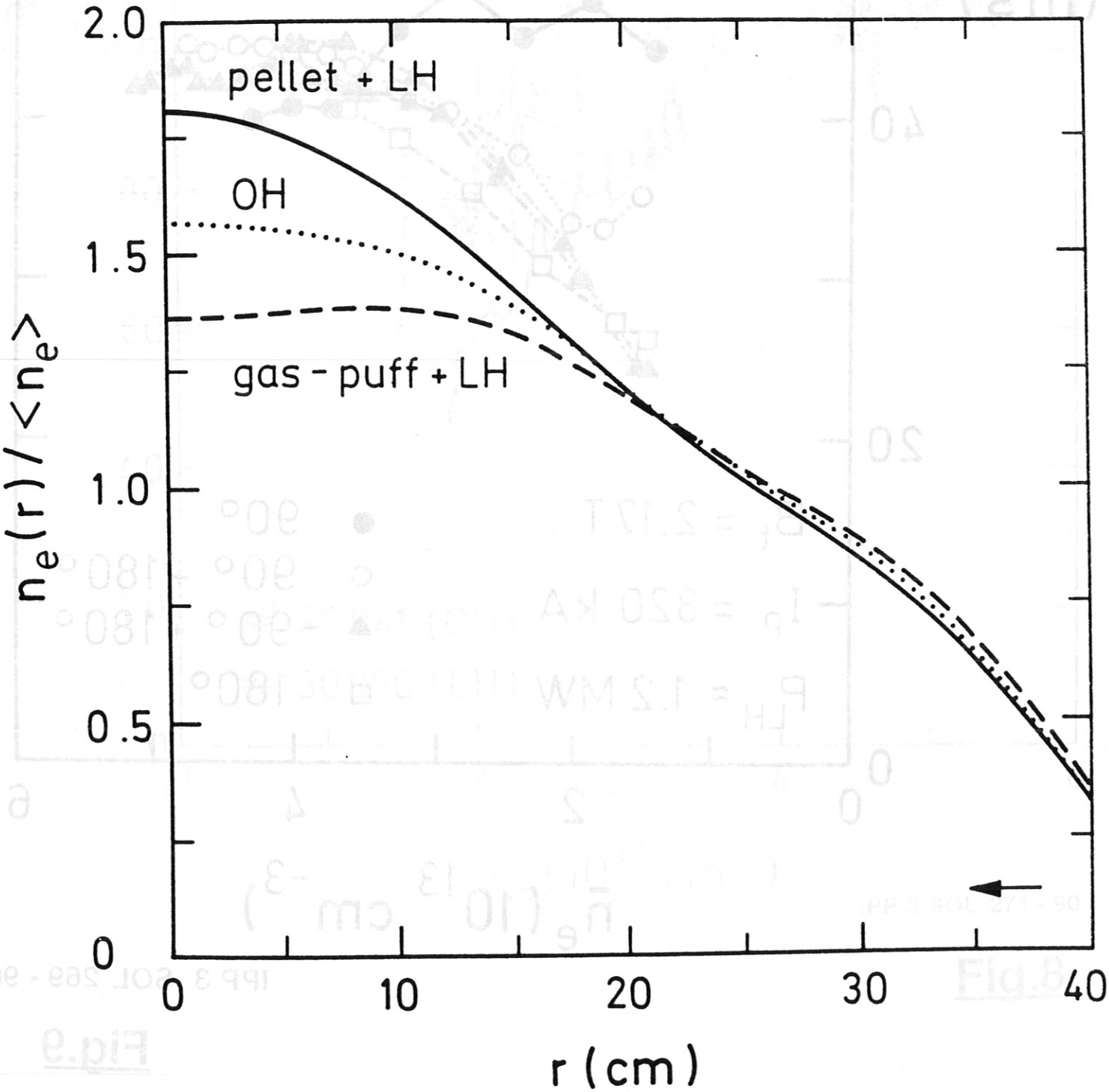


IPP 3 SOL 265 - 90

**Fig.10**

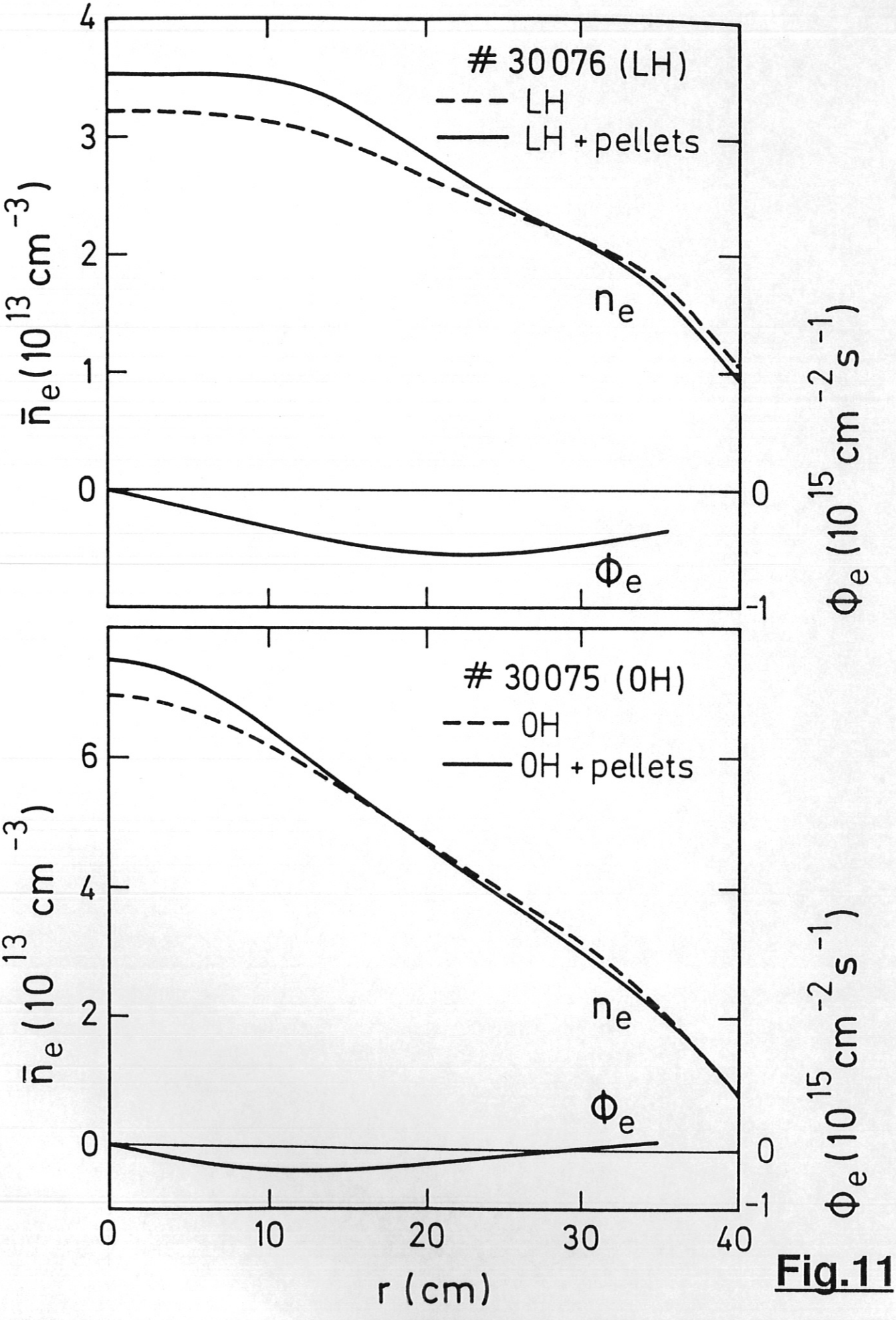
# 30076 (LH)
LH
LH + pellets
$n_e$
$\Phi_e$
$\bar{n}_e(10^{13}\,cm^{-3})$
$\Phi_e(10^{15}\,cm^{-2}s^{-1})$
# 30075 (OH)
OH
OH + pellets
$n_e$
$\Phi_e$
$\bar{n}_e(10^{13}\,cm^{-3})$
$\Phi_e(10^{15}\,cm^{-2}s^{-1})$
r (cm)

**Fig.11**